


Exploring the possible origin of the spin reorientation transition in NdCrO₃Hena Das ^{1,2,*} Alejandro F. Rébola ³ and Tanusri Saha-Dasgupta ⁴¹Laboratory for Materials and Structures, Tokyo Institute of Technology, 4259 Nagatesuta, Midori-ku, Yokohama, Kanagawa 226-8503, Japan²Tokyo Tech World Research Hub Initiative, Institute of Innovative Research, Tokyo Institute of Technology, 4259 Nagatsuta, Midori-ku, Yokohama, Kanagawa 226-8503, Japan³Instituto de Física Rosario - CONICET, Bv. 27 de Febrero 210 bis, S2000EKF Rosario, Santa Fe, Argentina⁴Department of Condensed Matter Physics and Material Sciences, S. N. Bose National Centre for Basic Sciences, JD Block, Sector III, Salt Lake, Kolkata, West Bengal 700106, India

(Received 24 August 2021; accepted 8 December 2021; published 27 December 2021)

Spin reorientation transitions and other related magnetic phenomena, which owe their origin to the complex interplay between multiple magnetic sublattices, have long attracted scientific attention both from the perspective of fundamental curiosity and technological applications. In this study, combining first principles calculations together with finite temperature Monte Carlo simulations, we explore the possible origins of reorientation transition of Cr spins in NdCrO₃. We construct a NdCrO₃ specific magnetic model, consisting of symmetric superexchange interactions between magnetic ions, as well as their magnetic anisotropy. We show that the observed spin reorientation in NdCrO₃ arises out of a delicate balance between Nd-Cr magnetic exchange interactions, single ion anisotropy of Nd spins, and single ion anisotropy of Cr spins. Moreover, though our model does not take into consideration the effect of antisymmetric and anisotropic-symmetric magnetic exchanges, the qualitative as well as quantitative agreement of the theoretically derived and the experimentally observed spin-reorientation transition in NdCrO₃ confirms the merit of our proposed microscopic model. Our results also propose a hitherto unobserved collective magnetic ordering in the Nd sublattice, which is challenging to detect as it is an extreme low temperature phenomena, which therefore calls for further investigations.

DOI: [10.1103/PhysRevMaterials.5.124416](https://doi.org/10.1103/PhysRevMaterials.5.124416)

I. INTRODUCTION

When multiple magnetic sublattices are formed in a perovskite structure, strong mutual interactions between these superlattices lead to unique magnetic and related phenomena [1–9]. The formation of these magnetic sublattices can be attributed to many factors, such as certain chemical compositions [10,11] or the formation of unique charge-ordered states [9]. In this regard, systems belonging to the rare-earth (R) transition metal (M) perovskite family, particularly RFeO₃ orthoferrites [4,5,12–15] and RCrO₃ orthochromites [6,16–25], exhibit a rich variety of magnetic properties resulting from the interplay of two different magnetic sublattices. These systems crystallize in the orthorhombic *Pbnm* structure. Though the magnetic properties of RCrO₃ compounds are similar to those of the isomorphous RFeO₃ ones, the former group exhibits a wider range of magnetic phase transitions depending on the characteristic features of the associated rare-earth ions [24,25]. The transition metal ordering temperatures are smaller by a factor ranging from two to six in the orthochromites compared to orthoferrites. For example, the M ordering temperature of NdFeO₃ is 690 K [12] as compared to that of NdCrO₃, which is reported to be 220 K [16]. This implies weaker M-M interaction in chromites compared to ferrites. Therefore, the M-M interaction in chromites is expected

to strongly compete with the other magnetic interactions, such as R-M and R-R interactions. Subtle changes in the relative strength of these magnetic interactions can therefore influence the nature of magnetic behavior. Here, we are interested in NdCrO₃, a system which was reported to show multiple phase transitions. However, the microscopic origin of these phenomena is yet to be deciphered. Moreover, for this system the magnitude of the rare-earth transition metal coupling is believed to be at least twice as large compared to its orthoferrite counterpart [17]. This phenomenon is also conjectured to influence the observed multiple phase transitions. However, the underlying microscopic mechanism is still unknown.

At high temperature, RMO₃ compounds are predominantly *G*-type antiferromagnets with small canting, which results in weak ferromagnetism [26,27]. A prominent phenomena in RMO₃ compounds is the spin reorientation (SR) [4,25], in which, as the temperature is lowered, the direction of the easy axis of the M sublattice magnetization changes from one crystal axis to another. Depending on the direction of the magnetization axis before and after the SR, six different groups can be identified [24]: (I) $G_x \rightarrow G_z$, (II) $G_x \rightarrow G_y$, (III) G_x , no SR, (IV) G_y , no SR, (V) $G_z \rightarrow G_y$, and (VI) G_z with a nonmagnetic R atom, no SR, where x , y , and z subscripts refer to easy-axis directions pointing to crystallographic a , b , and c directions, respectively. In the case of RCrO₃, the system corresponds to R = Ce, Sm, or Gd belonging to category (I), R = Er belongs to category (II), R = Y, La, or Eu belongs to category (III), R = Tb, Dy, Ho, Yb, Pr,

*das.h.aa@m.titech.ac.jp

or Tm belongs to category (IV), $R = \text{Nd}$ belongs to category (V), and $R = \text{Lu}$ belongs to category (VI). By contrast, the ferrite series shows less variety: the system corresponds to $R = \text{Pr, Nd, Sm, Tb, Ho, Er, Tm, or Yb}$ belonging to category (I), for $R = \text{Ce or Dy}$ belongs to category (II), and for $R = \text{Y, La, Eu, or Lu}$ belongs to category (III), in support of the fact that magnetism in chromites is more intricate and diverse compared to ferrites.

The magnetic properties of orthochromites and orthoferrites have been studied employing a variety of techniques, namely neutron diffraction and inelastic scattering [18,19], bulk magnetization and susceptibility measurements on powders and single crystals [28], specific-heat studies on powders and single crystals [17,29], Mossbauer effect [30], and optical-absorption spectroscopy [31]. In comparison, the theoretical studies are limited.

Within these systems, there are three types of magnetic interactions, $M^{3+}\text{-}M^{3+}$, $M^{3+}\text{-}R^{3+}$, and $R^{3+}\text{-}R^{3+}$, which according to their relative strengths set the following hierarchy: $M^{3+}\text{-}M^{3+} > M^{3+}\text{-}R^{3+} > R^{3+}\text{-}R^{3+}$ [24]. Each of these interactions generally consist of the isotropic, antisymmetric, and the anisotropic-symmetric superexchange interactions, apart from the single ion anisotropy of the M^{3+} and R^{3+} ions. This inevitably makes the theoretical study of magnetic properties of RMO_3 far from trivial. The most exhaustive study in this respect was carried out by Yamaguchi [24] in 1974, which employs first-order perturbation together with mean-field decoupling to study the spin-reorientation phenomenon in orthochromites and orthoferrites. In this work, the SR phenomena was investigated in the parameter space of a model Hamiltonian comprised of isotropic, antisymmetric, and the anisotropic-symmetric $M^{3+}\text{-}M^{3+}$, $M^{3+}\text{-}R^{3+}$ superexchange interactions, and the single-ion anisotropy of the M^{3+} ions. The magnetism of R sublattice was neglected, apart from M-R interaction. While this approach could explain the SR phenomena belonging to category (I) ($G_x \rightarrow G_z$) and category (II) ($G_x \rightarrow G_y$) highlighting the role of antisymmetric and anisotropic-symmetric $M^{3+}\text{-}R^{3+}$ interactions in SR of category (I) and category (II), the SR $G_z \rightarrow G_y$ [category (V)], as observed in NdCrO_3 , could not be explained.

The possible cause for the failure of this theory in explaining SR in category (V), involving Nd chromites, was speculated to be the single-ion anisotropy of Nd^{3+} , which was neglected in the theory by Yamaguchi [24], thus leaving the SR in NdCrO_3 unsolved. While the anisotropy energy of the Gd^{3+} ion is small enough to be neglected, and that of Dy^{3+} is large enough to be treated as an Ising spin, the anisotropy energy of Nd^{3+} is intermediate between the two. This may have an important influence in deciding SR in Nd chromites when the Nd-Cr interaction is not negligible. To the best of our knowledge, the interplay between the two has not yet been explored in the context of SR.

Nd chromite also appears to be a unique case in the context of Nd sublattice magnetism. Below the ordering temperature of the M sublattice, the Nd-M interaction has a tendency to polarize the Nd sublattice following the M sublattice ordering, thus acting as an effective magnetic field. Evidence of this is observed in Nd nickelates, ferrites, and chromites [17,32]. However, at sufficiently low temperature this coupling may compete with the weak R-R interaction and give rise to

cooperative long range ordering in the Nd sublattice. While existence of Nd sublattice ordering has been established in ferrites [29], the stronger Nd-M interaction in chromites puts in doubt/questions the existence of a cooperative magnetic ordering for the Nd sublattice of these systems. This behavior is counterintuitive since the M sublattice ordering temperature is lower in chromites compared to ferrites.

All the above issues make NdCrO_3 a challenging and interesting system which still remains to be understood. In the present study, we investigate the spin reorientation phenomena in NdCrO_3 by considering a spin Hamiltonian which consists of isotropic $M^{3+}\text{-}M^{3+}$, $M^{3+}\text{-}R^{3+}$, and $R^{3+}\text{-}R^{3+}$ superexchange together with single-ion anisotropy of both Nd^{3+} and Cr^{3+} sites. We employ state-of-the-art first-principles density functional theory (DFT) calculations to extract the parameters of the spin Hamiltonian relevant for NdCrO_3 . The parameters extracted from DFT calculations and based on the experimentally measured crystal structure of NdCrO_3 encode the structural and chemical details of the system. Subsequently, the finite temperature magnetic properties of the spin Hamiltonian were obtained by Monte Carlo simulations considering the spin Hamiltonian. Our results reveal that such a Hamiltonian is able to capture the spin reorientation in NdCrO_3 correctly. The calculated transition temperatures corresponding to the Néel ordering of Cr spins and SR are in reasonable agreement with experimental values. Our study pinpoints the interplay of the M-M and M-R interactions and single-ion anisotropy of Nd and Cr sites in driving this exceptional SR phenomena. Since we are primarily interested in the study of SR and in the role of single-ion anisotropy, this study does not take into account the antisymmetric and the anisotropic-symmetric superexchange interactions, which would give rise to noncollinear magnetism of Cr spins resulting in a small canting, as reported experimentally.

Moreover, our first principles study combined with Monte Carlo simulations unravel a yet unreported C-type magnetic ordering in the Nd sublattice, throwing further debate on the nature of cooperative ordering of Nd spins in NdCrO_3 . Further experimental studies as well as theoretical ones taking into account the influence of antisymmetric and anisotropic-symmetric superexchange interactions are needed to settle the issue conclusively.

The present work underlines the effectiveness of first-principles calculations in capturing the complexity of rare earth transition metal oxides involved in the delicate balance between magnetic interactions and single ion anisotropies of two of the magnetic sublattices. It further establishes the power of such an approach in providing a microscopic understanding of SR transition in NdCrO_3 , a phenomenon that still remains unsolved by the theory.

II. COMPUTATIONAL DETAILS

Using the experimentally determined $Pbnm$ crystal structures, the symmetric exchange interactions between the magnetic ions as well as their magnetic anisotropy parameters were estimated through the calculation of total energy of various collinear magnetic configurations employing the density functional theory (DFT) based linearized augmented plane-wave (LAPW) method as implemented in the WIEN2K code

[33,34]. We considered 16 magnetic configurations in order to estimate the strength of the symmetric exchange interactions and six magnetic configurations to estimate the magnetic anisotropy parameters of the ions. We used the Perdew-Burke-Ernzerhof (PBE) [35] generalized gradient approximation (GGA) form of the exchange correlation functional. The effect of the missing correlation on the transition metal Cr sites (with localized $3d$ electrons) and rare earth Nd sites (with localized $4f$ electrons) beyond the GGA was taken into account through supplemented Hubbard U and Hund's coupling J_H terms using the GGA+ U method [36]. The choice of appropriate U and J_H values, for that matter, is very crucial in quantitative description of the magnetic and electronic structures of strongly correlated insulators like the system in question. Following the values of U estimated by employing the constrained density functional theory (cDFT) method [37] and previous theoretical studies [8,38], we performed our calculations considering U for Cr in the range of 2–5.5 eV (0.15–0.40 Ryd). On the other hand, we set a 5.5 eV (0.40 Ryd) value of U at the Nd site. This strategy gave us the opportunity to study the effect of the relative strength of U at the Cr and Nd sites on the properties of NdCrO_3 . Additionally, we considered a range of values, 0–1.0 eV, for the J_H parameter, a factor which is found to have a strong influence on the estimated magnetic parameters. We performed our calculations using a plane-wave cutoff of $RK_{MAX} = 7$ and Monkhorst-Pack Γ centered k -point mesh of $6 \times 6 \times 4$ for $Pbnm$ structure. We also considered $1 \times 2 \times 1$ and $2 \times 1 \times 1$ supercell structures to estimate R-M magnetic interactions and the corresponding k -point meshes were of the dimensions $6 \times 4 \times 4$ and $4 \times 6 \times 4$, respectively.

Employing METROPOLIS algorithms [39,40] and periodic boundary conditions as implemented in our group MC package, classical Monte Carlo (MC) simulations were performed to study magnetic phase transition as a function of temperature. In order to calculate total energy $\xi(T)$ as a function of temperature (T), we considered N_{MC} MC steps for each temperature step and performed $N_{\text{ion}} = N_{Cr} + N_{Nd}$ spin flips. Here N_{Cr} and N_{Nd} denote the total number of Cr and Nd ions, respectively, in the MC supercell structure. Each spin flip randomly rotates the direction of the selected spin with a uniform probability distribution of the associated unit spin vector over a unit sphere. We calculated specific heat as a function of temperature using

$$C_v(T) = \frac{\langle \xi(T)^2 \rangle - \langle \xi(T) \rangle^2}{k_B T^2}, \quad (1)$$

where the angle brackets denote thermal average.

We report the results of Monte Carlo (MC) simulations performed on an $8 \times 8 \times 8$ cell consisting of 4096 magnetic ions, and considering 10^9 MC steps for each temperature using the model Hamiltonian constructed through GGA+ U calculations. The convergence of $\xi(T)$ and the ground state magnetic structure was cross-checked by considering up to $10 \times 10 \times 10$ ($N_{\text{ion}} = 8000$) cell size and 10^9 MC steps. We considered the cooling process to investigate the stability of the magnetic phases. During this process, the final simulated magnetic configuration corresponding to a particular temperature was considered as the initial magnetic configuration corresponding to the next value of temperature. In addition, we conducted finite temperature MC simulations further con-

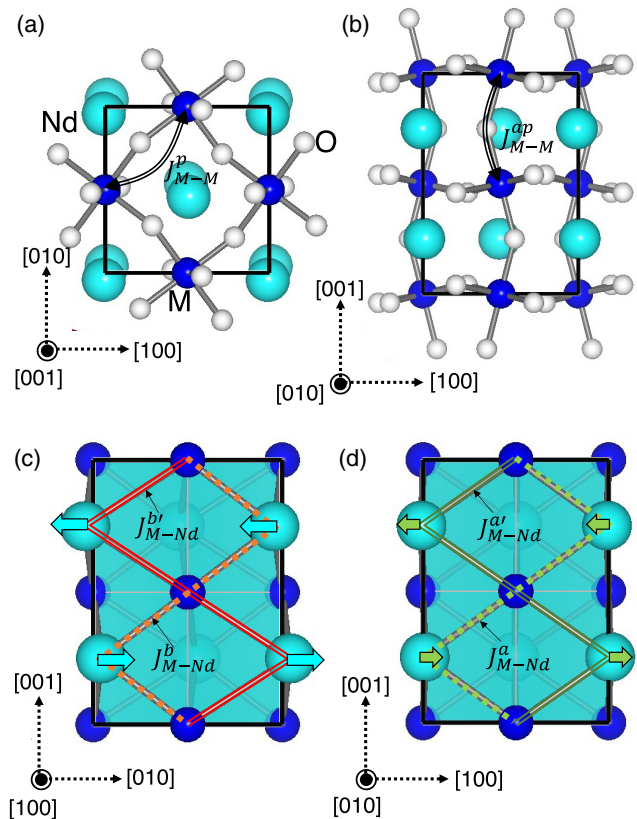


FIG. 1. Orthorhombic $Pbnm$ crystal structure of NdCrO_3 . Crystal structure showing the first nearest-neighbor isotropic M-M exchange interactions, in plane (J_{M-M}^p) (a) and out of plane (J_{M-M}^{ap}) (b). Crystal structure plot exhibiting four in-equivalent NN M-Nd exchange interactions, denoted as J_{M-Nd}^b and $J_{M-Nd}^{b'}$ (in the crystallographic bc plane) (c) and J_{M-Nd}^a and $J_{M-Nd}^{a'}$ (in the crystallographic ac plane) (d). The arrows indicate the antiferro off-centric displacements of Nd ions.

sidering a wide variation in the magnetic parameter range of R-M superexchanges, and single ion anisotropy of M ions beyond the DFT estimated values, to unravel and identify the driving forces behind the complex magnetic behavior of NdCrO_3 . In order to determine the primary collinear G -type AFM phase in the Cr sublattice, we calculated the magnetic order parameter defined as

$$[m_a, m_b, m_c] = \langle \mathbf{S}_1 - \mathbf{S}_2 + \mathbf{S}_3 - \mathbf{S}_4 \rangle / 4S, \quad (2)$$

where $\mathbf{S}_1 \rightarrow \mathbf{S}_4$ represent four Cr ($S = 3/2$) ions in the $Pbnm$ unit cell. m_a , m_b , and m_c denote the staggered moments along the crystallographic a , b , and c axis, respectively.

III. RESULTS

A. Crystal structure

The NdCrO_3 compound crystallizes in the orthorhombic $Pbnm$ space group, which is the GdFeO_3 -type distorted perovskite structure with both an in-phase and out-of-phase CrO_6 octahedral tilting distortion pattern of $a^- a^- c^+$, as shown in Figs. 1(a) and 1(b). The lattice constants of the orthorhombic unit cell were measured as [41]

$a = 5.421$ Å, $b = 5.487$ Å, and $c = 7.694$ Å. The experimentally determined Wyckoff positions corresponding to Nd, Cr, O_{ap} (apical oxygen), and O_p (planar oxygen) ions are $4c$ ($x, y = -0.009, 0.042$), $4b$, $4c$ ($x, y = 0.089, 0.480$), and $8d$ ($x, y, z = -0.287, 0.285, 0.040$), respectively. The resultant orthorhombic distortion, measured as $\frac{2 \times (b-a)}{(b+a)}$, is 0.012. In addition to rotation $a^0 a^0 c^+$ (M_3^+) and tilt $a^- a^- c^0$ (R_4^+) distortions, Nd ions exhibit antiferro off-centric displacements along the crystallographic a and b axes, following the R_5^+ [Fig. 1(c)] and X_5^+ [Fig. 1(d)] symmetries, respectively. This leads to the formation of Nd-Cr short bonds (3.165 Å and 2.293 Å) and long bonds (3.370 Å and 3.540 Å), respectively. We considered this crystal structure in order to conduct the first-principles electronic structure calculations and to construct the magnetic model Hamiltonian to perform finite temperature Monte Carlo simulations. Considering the fact that no significant change in orthorhombic distortion was reported below the Néel temperature (T_N) [41], we kept the crystal structure fixed in the temperature range of the Monte Carlo simulations.

B. Model Hamiltonian

To investigate the magnetic phase transitions in NdCrO₃ at finite temperatures we constructed a magnetic model Hamiltonian comprised of isotropic exchange interactions between the magnetic ions and the magnetic anisotropy energies of the magnetic ions. The isotropic exchange component of the Hamiltonian is given by

$$H_{SE} = H_{M-M} + H_{M-Nd} + H_{Nd-Nd}, \quad (3)$$

where

$$H_{M-M} = \sum_{\langle i_1, j_1 \rangle_c} J_{M-M}^{ap} \mathbf{S}_{i_1} \cdot \mathbf{S}_{j_1} + \sum_{\langle i_1, j_1 \rangle_{ab}} J_{M-M}^p \mathbf{S}_{i_1} \cdot \mathbf{S}_{j_1} + \sum_{\langle i_1, j_1 \rangle_{NNN}} J_{M-M}^{NNN} \mathbf{S}_{i_1} \cdot \mathbf{S}_{j_1} \quad (4)$$

represents the nearest-neighbor (NN) isotropic exchange interactions between M spins (denoted by \mathbf{S}) mediated via apical (J_{M-M}^{ap}) and planar (J_{M-M}^p) oxygen [cf. Figs. 1(a) and 1(b)] and their next-nearest-neighbor (NNN) interactions (J_{M-M}^{NNN}). In Eq. (4), i_1 and j_1 denote the site of the M spins. The $\langle i_1, j_1 \rangle_c$ and $\langle i_1, j_1 \rangle_{ab}$ represent the sum over NN M-M pairs along the crystallographic c axis and in the crystallographic ab plane, respectively. And the sum $\langle i_1, j_1 \rangle_{NNN}$ goes over NNN M-M pairs. We counted every pair once.

The most important interactions are between two magnetic sublattices and the associated energy component is given by

$$H_{M-Nd} = \sum_{\langle i_1, i_2 \rangle_1} J_{M-Nd}^b \mathbf{S}_{i_1} \cdot \mathbf{S}'_{i_2} + \sum_{\langle i_1, i_2 \rangle_2} J_{M-Nd}^{b'} \mathbf{S}_{i_1} \cdot \mathbf{S}'_{i_2} + \sum_{\langle i_1, i_2 \rangle_3} J_{M-Nd}^a \mathbf{S}_{i_1} \cdot \mathbf{S}'_{i_2} + \sum_{\langle i_1, i_2 \rangle_4} J_{M-Nd}^{a'} \mathbf{S}_{i_1} \cdot \mathbf{S}'_{i_2}, \quad (5)$$

which incorporates the effect of the orthorhombic displacement of the Nd ions, resulting in four inequivalent exchange interactions: J_{M-Nd}^b , $J_{M-Nd}^{b'}$, J_{M-Nd}^a , and $J_{M-Nd}^{a'}$ [cf. Figs. 1(c) and 1(d)]. \mathbf{S}' denotes Nd spin and i_2 represents the Nd site. The $\langle i_1, i_2 \rangle_{1 \rightarrow 4}$ run over NN M-Nd pairs. The first pair of

interactions corresponds to the short M-Nd bond connections, while the second pair represents the same along the longer M-Nd bonds. Here we define a parameter γ which denotes the strength of the strongest NN isotropic exchange interaction between two magnetic sublattices J_{M-Nd} relative to the strongest exchange interaction between M spins J_{M-M} , i.e.,

$$\gamma = \frac{J_{M-Nd}}{J_{M-M}}.$$

In addition, we considered the NN isotropic exchange interactions between the Nd spins along the three crystallographic axes, denoted as J_{Nd-Nd}^a , J_{Nd-Nd}^b , and J_{Nd-Nd}^c , respectively. The corresponding energy term is given by

$$H_{Nd-Nd} = \sum_{\langle i_2, j_2 \rangle_a} J_{Nd-Nd}^a \mathbf{S}'_{i_2} \cdot \mathbf{S}'_{j_2} + \sum_{\langle i_2, j_2 \rangle_b} J_{Nd-Nd}^b \mathbf{S}'_{i_2} \cdot \mathbf{S}'_{j_2} + \sum_{\langle i_2, j_2 \rangle_c} J_{Nd-Nd}^c \mathbf{S}'_{i_2} \cdot \mathbf{S}'_{j_2}, \quad (6)$$

where i_2 and j_2 represent Nd sites. The $\langle i_2, j_2 \rangle_a$, $\langle i_2, j_2 \rangle_b$, and $\langle i_2, j_2 \rangle_c$ sum over the NN Nd-Nd pairs (each pair is counted once) along the crystallographic a , b , and c axis, respectively.

The magnetic anisotropy of the system was modeled by considering the single ion anisotropy (SIA) energies of the M and Nd ions. The corresponding component of the spin Hamiltonian is given by

$$H_{SIA} = \sum_{i_1} \{ E_M (S_{i_1x}^2 - S_{i_1y}^2) + D_M S_{i_1z}^2 \} + \sum_{i_2} [E_{Nd} \{ (S'_{i_2x})^2 - (S'_{i_2y})^2 \} + D_{Nd} (S'_{i_2z})^2]. \quad (7)$$

The x , y , and z directions correspond to the crystallographic a , b , and c axes, respectively, of the $Pbnm$ structure. For ($E < 0, D < 0, |E| > |D|$) and ($E < 0, D > 0$) conditions, the spins tend to orient along the x (crystallographic a) axis. On the other hand, ($E < 0, D < 0, |E| < |D|$) and ($E > 0, D < 0, |E| < |D|$) denote the preference of spins to orient along the z (crystallographic c) axis. Finally, ($E > 0, D < 0, |E| > |D|$) and ($E > 0, D > 0$) tend to orient the spins along the y (crystallographic b) axis. The analysis based on site symmetries of both Cr and Nd ions shows the possible existence of nonzero off-diagonal components of the associated SIA tensors in addition to the nonzero diagonal components. However, in the present study, we have taken only the latter into consideration.

C. DFT electronic structure

Figure 2(a) shows the electronic structure of NdCrO₃ computed within GGA+ U formalism and considering a G -type antiferromagnetic order in both the Nd and Cr sublattice. The results presented in the following are for the choice of $U_{Cr} = 2.2$ eV, $U_{Nd} = 5.5$ eV, and $J_H = 0.3$ eV, which were found to provide the best description of magnetic moments and exchange interactions in relation to the experimental observations. The system shows insulating behavior with an ~ 2.5 eV band gap. The approximate octahedral oxygen environment surrounding Cr ions splits the $3d$ states into t_{2g} and e_g manifolds. The t_{2g} manifold is filled (empty) in the majority (minority) spin channel for Cr, indicating a nominal 3+ valence state as reported in orthochromites. The electron

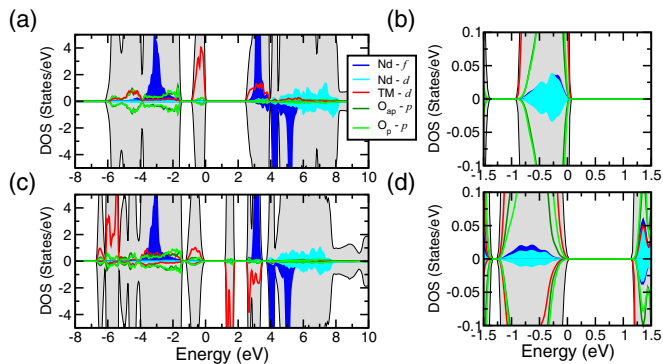


FIG. 2. (a),(c) Calculated density of states (DOS) for NdCrO₃ and NdFeO₃ considering collinear *G*-type antiferromagnetic order in the Cr sublattice as well as the Nd sublattice. The Nd-Cr and Nd-Fe hybridization are highlighted in zoomed plots (b) and (d). We considered $U = 2.2$ eV and $J_H = 0.3$ eV for Cr 3*d* states and $U = 4.5$ eV and $J_H = 0.3$ eV for Fe 3*d* states. A higher U value of 5.5 eV and $J_H = 0.3$ eV for Nd 4*f* states was used.

occupancy of the Nd-4*f* orbitals also indicates a 3+ valence state. The values of the calculated spin moments at Cr and Nd sites are $\sim 2.52 \mu_B$ and $\sim 2.96 \mu_B$, respectively. These spin moments provide additional support to the nominal 3+ valences at both transition metal (M) and rare-earth (R) sites. The 4*f* electrons of Nd are coupled with its 5*d* electrons by the intra-atomic exchange interaction. Also, since the 5*d* orbitals are spatially extended, they hybridize with the M-3*d*. This hybridization has been clearly depicted in the zoomed plot in Fig. 2(b), which shows a strong overlap between the Nd-5*d*-4*f* and the Cr-3*d* states. For comparative analysis, we also calculated the electronic structure of the *G*-type ordered magnetic phase of NdFeO₃ considering $U = 4.5$ eV and $J_H = 0.3$ eV at the Fe 3*d* states, presented in Figs. 2(c) and 2(d). As in the case of orthochromites, in this orthoferrite too, both Fe and Nd ions tend to favor the formation of a +3 valence state. Very interestingly, we find that the integrated DOS of Nd-5*d* in the energy range of -1.5 eV to Fermi level is approximately two times higher in NdCrO₃ compared to that in NdFeO₃, which indicates that the Nd-Cr hybridization is about two times stronger than the Nd-Fe hybridization. This relation is in good line with the experimentally observed relation (based on the specific heat and neutron-diffraction measurements [17]) between the values of the mean-field Nd-Cr and Nd-Fe interaction parameters (n_{M-R}), where the former is 2.6 times that of the latter.

D. Estimated isotropic exchange interactions

We estimated the values of the isotropic exchange interactions between magnetic ions of NdCrO₃ using the calculated total energies of 16 spin configurations and the results are listed in Table I for $J_H = 0.3$ eV and the U value of 2.2 eV and 5.5 eV corresponding to the Cr 3*d* and Nd 4*f* states, respectively. Additionally, we conducted the calculations considering a range of U and J_H values. The results are summarized in Figs. S1 and S2 (Supplemental Material [42]). We estimated the values of exchange interactions considering the spin value of 3/2 for both Cr and Nd. The strongest

TABLE I. Estimated values of isotropic exchange interactions and SIA parameters using $U = 2.2$ eV and 5.5 eV for the transition metal Cr 3*d* and rare-earth 4*f* states, respectively, and $J_H = 0.3$ eV.

Isotropic exchange (meV)							
System	J_{M-M}^p	J_{M-M}^{ap}	J_{M-M}^{mm}	J_{M-Nd}^b	$J_{M-Nd}^{b'}$	J_{M-Nd}^a	$J_{M-Nd}^{a'}$
NdCrO ₃	4.66	6.01	0.09	2.63	-2.08	0.84	-0.23
SIA (meV)							
System	E_{Nd}	D_{Nd}	E_M	D_M			
NdCrO ₃	-0.40	-0.10	0.003	-0.01			

interaction, $J_{Cr-Cr} = 6.01$ meV, corresponds to the antiferromagnetic (AFM) NN interaction between Cr spins mediated via the apical oxygens. The Cr spins are also coupled antiferromagnetically in the *ab* plane, leading to the stabilization of the *G*-type AFM phase, which is in agreement with the experimental observations [3]. The estimated average value of the NN Cr-Cr interaction 5.11 meV (~ 59 K) is in close agreement with the experimentally determined [17] value of 44 K. The NNN interactions are comparatively weak and AFM in nature with an average value of ~ 0.09 meV, which is expected to cause weak magnetic frustration in the Cr sublattice. The values of the NN exchange interactions increase linearly with the increase of J_H [see Fig. S1(a) in the Supplemental Material [42]].

The interactions between two magnetic sublattices significantly vary with the value of J_H , as shown in Fig. S1(b) (Supplemental Material [42]). The orthorhombic distortions result in AFM and FM interactions between the Nd and Cr spins along the shorter and longer bond directions, respectively. We observe that $|J_{Cr-Nd}^b - J_{Cr-Nd}^{b'}| > |J_{Cr-Nd}^a - J_{Cr-Nd}^{a'}|$, implying that the difference in magnetic interactions due to antiferro off-centric displacements of Nd ions along the crystallographic *b* axis is higher than that along the crystallographic *a* axis. Interestingly, the displacement of the Nd ions along the *b* axis (Q_b) is higher in order of magnitude compared to that along the *a* axis (Q_a). Thus the orthorhombic separation between magnetic interactions directly vary with the amplitude of the off-center displacement of the Nd ions. The strongest interaction corresponds to AFM $J_{Cr-Nd} = J_{Cr-Nd}^b = 2.63$ meV, which gives rise to the relative strength of $\gamma = 0.44$. This relative strength varies from 0.25 to 0.89 as we vary the J_H value from 0 to 1.0 eV (see Fig. S2 in the Supplemental Material [42]). This indicates a strong correlation between the exchange interactions between the two magnetic sublattices and J_H . The average exchange interaction (J_{Cr-Nd}^{avg}) between two magnetic sublattices is AFM in nature, which is in line with the experimental observation [18]. It is important to point out here that a similar exercise carried out for NdFeO₃ with $U = 4.5$ eV and $J_H = 0.3$ eV at the Fe site gave a γ value of 0.25, a factor of 1.8 smaller compared to NdCrO₃, in good agreement with our conclusions on relative Nd-M hybridization between chromites and ferrites from density of states as well as that concluded from specific heat measurement [17].

In addition, we also estimated the magnetic interactions between Nd spins, which were found to be weak and AFM in nature along all three crystallographic axes with an average

value of 0.02 meV, indicating a G -type magnetic order in the Nd sublattice. However, these interactions are of an order of magnitude weaker than the magnetic interactions between two sublattices.

E. Estimated single ion anisotropy (SIA)

Next, we calculated the magnetic anisotropy energy of the Nd ions, and the results are given in Table I. In order to decouple the contribution of the Cr spin sublattice, we only employ spin-orbit (LS) coupling at the Nd spins. As the electronic configuration of $R-4f$ electrons follows Hund's rule, the orbital magnetic moment appears in the presence of spin-orbit coupling (SOC). Once the direction of the $4f$ orbital moment gets fixed, the direction of the spin moment also gets fixed by the LS coupling. The anisotropy energies, $\Delta E'_a$ and $\Delta E'_b$ [as defined in Fig. S3(a) in the Supplemental Material [42]], were calculated by considering spin configurations oriented along the crystallographic a (x), b (y), and c (z) axes. Employing calculated magnetic anisotropy energies and Eq. (7) we estimated the values of E_{Nd} and D_{Nd} as $E_{Nd} = \frac{\Delta E'_a - \Delta E'_b}{2(S')^2}$ and $D_{Nd} = -\frac{\Delta E'_a + \Delta E'_b}{2(S')^2}$. We observed that, irrespective of the value of J_H , the anisotropy energy associated with the orientation of Nd spins along the crystallographic b axis is higher than the corresponding energies along the crystallographic a and c axes [see Fig. S3(a) in the Supplemental Material [42]]. Our calculations show that the Nd sublattice exhibits biaxial magnetic anisotropy, where the easy and intermediate magnetic axes are along the crystallographic a and c axes, respectively, and the magnetic hard axis is along the crystallographic b axis [see Table I and Fig. S3(a) in the Supplemental Material [42]]. The calculated orbital moment of Nd $\sim 1.63 \mu_B$ and is oriented antiparallel to the spin moment. The net magnetic moment $\mu_{Nd} \sim 1.33 \mu_B$, lying well within the experimentally reported range of 1.30–1.93 μ_B [18,19]. We notice here $J_{Cr-Nd}^{\text{avg}} = 0.29$ meV, comparable to DFT estimated SIA of Nd spins, hinting into a strong interplay between the two.

Compared to the magnetic anisotropy energies of the Nd ions, the anisotropy energies of the Cr ions are an order of magnitude lower (see Fig. S3 in the Supplemental Material [42]). To obtain the magnetic anisotropy of the Cr ions (ΔE_a and ΔE_b), we switch on the LS coupling only for the Cr ions. The values of E_{Cr} and D_{Cr} were estimated using $E_{Cr} = \frac{\Delta E_a - \Delta E_b}{2S^2}$ and $D_{Cr} = -\frac{\Delta E_a + \Delta E_b}{2S^2}$. The computed orbital moment at the Cr site $\sim 0.03 \mu_B$. As shown in Fig. S3(b) in the Supplemental Material [42], Cr tends to orient along the crystallographic c axis and this tendency enhances with the increase in J_H . This observation agrees with the experimentally observed stabilization of the G_z magnetic phase below Néel temperature [18]. However, the weak magnetic anisotropy of the Cr spins is expected to be associated with high numerical error. We, therefore, scan the stability of the magnetic phases in NdCrO_3 as a function of the SIA parameters of the Cr spins (E_{Cr} , D_{Cr}) employing finite temperature Monte Carlo simulations.

F. Finite temperature Monte Carlo simulations

Monte Carlo (MC) simulations were performed using the model Hamiltonian constructed with the U values of 2.2 eV

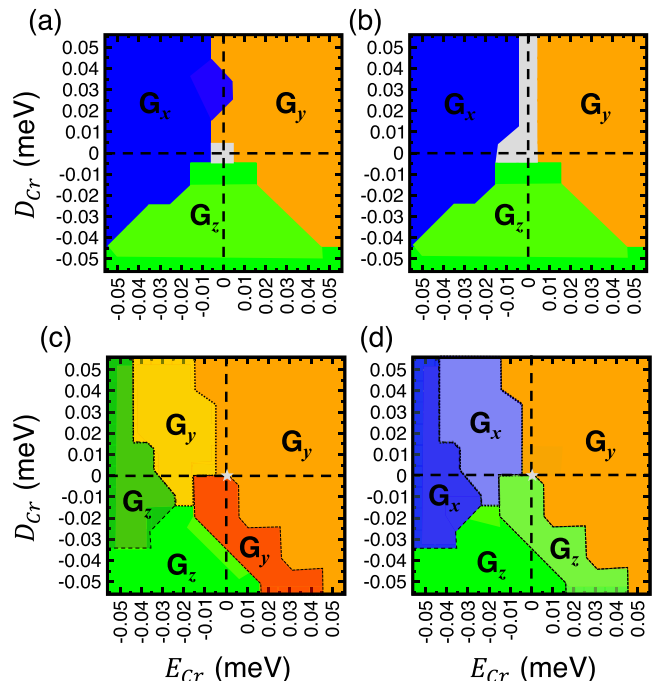


FIG. 3. Observed collective spin ordering in the Cr sublattice at 5 K (a) and 75 K (b) as a function of E_{Cr} and D_{Cr} for $|E_{Nd}| = |D_{Nd}| = 0$. We performed MC simulations considering $E_{Cr} \neq 0$ and $D_{Cr} \neq 0$, as the $E_{Cr} = D_{Cr} = 0$ case leads to huge degeneracy. The same for GGA+ U estimated values of E_{Nd} and D_{Nd} at 5 K (c) and 75 K (d). G_x , G_y , and G_z denote orientation of Cr spins along the crystallographic a , b , and c axes, respectively. Different phases are shaded with different colors. The color coding is the same between 5 K and 75 K, if there is no change in symmetry of spin ordering of Cr spins and shaded differently when there is a change in symmetry of spin ordering of Cr spins between 5 K and 75 K. The values of isotropic magnetic exchanges are kept fixed at GGA+ U estimated values obtained with the choice of $J_H = 0.3$ eV. In the parameter region shaded with light gray, none of the following phases, G_x , G_y , and G_z , are formed.

and 5.5 eV at the Cr $3d$ and Nd $4f$ states, respectively, and $J_H = 0.3$ eV. This set of particular values of U and J_H were taken into consideration, since the magnetic properties of the material, when calculated using this particular set, were in best agreement with the experimentally obtained results [16–18]. The primary motivation of the present study is to explore the interplay between isotropic Nd-Cr exchange interactions and SIA, which can induce the spin-reorientation transitions. With this motivation in mind, we first explore the parameter space of SIA, (E_{Nd} , D_{Nd}) and (E_{Cr} , D_{Cr}).

Case: $E_{Nd} = D_{Nd} = 0$. We start our discussion by considering the MC simulation results where the magnetic anisotropy of the Nd ions is switched off ($E_{Nd} = D_{Nd} = 0$) and the magnetic anisotropy of Cr ions is varied from -0.05 to 0.05 meV. Figures 3(a) and 3(b) show the observed magnetic order in the Cr sublattice at 5 K and 75 K, respectively, as a function of E_{Cr} and D_{Cr} . Note that we conducted MC simulations considering $E_{Cr} \neq 0$ and $D_{Cr} \neq 0$, as the $E_{Cr} = D_{Cr} = 0$ case leads to huge degeneracy due to spherical symmetry. We determined the order by calculating the staggered magnetization as defined in Eq. (2). Irrespective of the value of E_{Cr} and

D_{Cr} , the specific heat, calculated as a function of temperature, shows a peak at around 172 K, indicating a magnetic transition from the paramagnetic phase to a G -type AFM phase in the Cr sublattice and a disordered state in the Nd sublattice. Depending on the parameter values of E_{Cr} and D_{Cr} , G_x or G_y or G_z phase is stabilized in the Cr sublattice. Comparison between Figs. 3(a) and 3(b) reveals no spin-reorientation transition of the Cr spins was observed down to 5 K. This provides the key finding of our study that for SR in the Cr sublattice the SIA of Nd ions plays a crucial role.

Case: $E_{Nd} \neq 0, D_{Nd} \neq 0$. Figures 3(c) and 3(d) summarize the results of MC simulations considering the DFT estimated values of SIA E_{Nd} and D_{Nd} parameters (see Table I). The main findings are as follows. (1) The calculated specific heat for a temperature range of 300–5 K shows two peaks. One at around 172 K and another at around 11 K. The first transition temperature corresponds to Néel temperature (T_N) forming G -type Cr spin order. The T_N value remained unchanged between $E_{Nd} = D_{Nd} = 0$ and $E_{Nd} \neq 0, D_{Nd} \neq 0$, indicating that high temperature magnetic ordering of the Cr sublattice does not depend on the Nd sublattice. However, contrary to the $E_{Nd} = D_{Nd} = 0$ case, SR transition is observed in the Cr sublattice depending on the choice of E_{Cr}, D_{Cr} [compare Figs. 3(c) and 3(d)]. The existence and precise nature of the SR transition is found to strongly depend on the value of Cr SIA parameters, as depicted in various shaded regions in Figs. 3(c) and 3(d). (2) For the choice of (E_{Cr}, D_{Cr}) parameters within a critical range, as shown by the region shaded in red in Fig. 3(c), a reorientation of the G -type ordered Cr spins from z to y axis ($G_z \rightarrow G_y$) at 11 K is observed, which corresponds to the experimentally reported spin reorientation transition observed in NdCrO₃ [17]. (3) Additionally, our results highlight a comprehensive correlation between the magnetic anisotropy of the magnetic ions and the nature of SR transitions in the Cr sublattice. The Cr spins, notably, either orient along the y or the z axis, below the second magnetic transition temperature. The strong tendency of the Nd spins to be oriented along the x axis exclude the formation of the G_x magnetic phase.

The DFT estimated SIA coefficients of Cr ions are $E_{Cr} = 0.003$ meV and $D_{Cr} = -0.01$ meV, which lie in the critical parameter space that leads to the $G_z \rightarrow G_y$ spin-reorientation transition at the second transition temperature. Two noteworthy points in this regard are (I) the $G_z \rightarrow G_y$ SR transition takes place for $D_{Cr} < 0$, i.e., when the magnetic easy axis of the Cr sublattice is along the crystallographic c axis, which is in line with the observed trend of magnetic anisotropy of Cr ions through DFT calculations, and (II) based on our present mechanism, SR transitions occur if the magnetic easy axis of the Cr sublattice coincides with one of the easy axes of the Nd sublattice and due to the strong Cr-Nd superexchange interactions below SR transition temperature (T_{SR}) Cr spin orient along the magnetic hard axis of the Nd sublattice. The calculated T_N and T_{SR} [see Fig. 4(a)] are in the same ballpark but somewhat underestimated compared to the experimentally reported values of 224 K and 34 K [17], respectively. The present model, however, excludes the effect of anisotropic and antisymmetric exchange interactions, which can influence the precise values of the magnetic transition temperatures. The magnetic exchanges and SIA being strongly dependent on the choice of J_H value provides another avenue of fine-tuning of

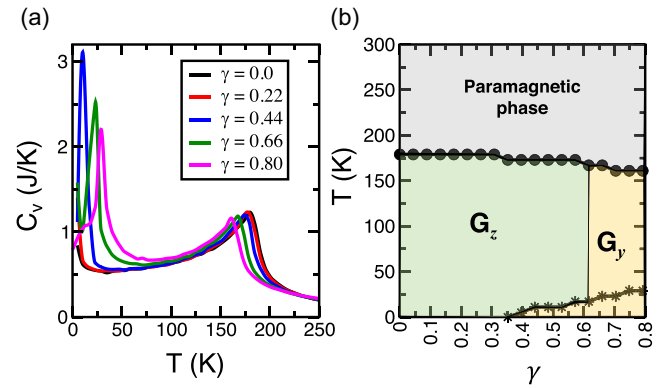


FIG. 4. (a) Calculated temperature dependence of specific heat for a choice of γ values. We used $E_{Cr} = 0.02$ meV and $D_{Cr} = -0.05$ meV. Though the nature of magnetic phase transitions strongly depends on the magnetic anisotropy of Nd and Cr ions, the value of transition temperatures shows weak dependence. (b) Magnetic phase diagram in T - γ plane, demarcating the paramagnetic, G_z and G_y spin ordered phases of the Cr sublattice. The calculated Néel temperature T_N values, plotted in solid circles, denote paramagnetic to G -type AFM ordering temperature, while the second transition temperature is plotted in stars. For $\gamma \sim 0.35$ – 0.62 , stars denote $G_z \rightarrow G_y$ SR transition.

the transition temperatures, which we refrain from doing as our motivation is to unravel the origin rather than provide a perfect match with experimental transition temperatures.

In order to further explore the correlation between the relative strength of the exchange interactions between the two magnetic sublattices and the SR transitions, we carried out additional MC simulations as a function of γ keeping the DFT determined relative strength of all four Cr-Nd interactions fixed. The $\gamma \sim 0.44$ case corresponds to the DFT estimated parameters. The calculated Cr sublattice staggered magnetization as a function of γ is shown in Fig. S4(b) in the Supplemental Material [42]. Our results demonstrate the existence of a second transition only above a critical value of $\gamma = 0.35$, as shown in Fig. 4(a). While the value of Néel temperature decreases with the increase of γ , the value of the second transition temperature increases. As shown in the γ - T phase diagram in Fig. 4(b) and Fig. S4(b) in the Supplemental Material [42], within a range of $\gamma \sim 0.35$ – 0.62 , NdCrO₃ is found to show $G_z \rightarrow G_y$ SR transition. For $\gamma > 0.62$, the second transition corresponds to the spin ordering in the Nd sublattice and not to SR transition of the Cr sublattice.

The above exercise conclusively establishes that the SR transition of NdCrO₃ is a complex interplay of Nd-Cr magnetic exchanges, SIA of the Nd and Cr sublattices. On the other hand, we also studied the magnetic phase transitions in NdFeO₃ using the GGA+ U estimated value of γ , isotropic superexchange interactions between Fe spins, and magnetic anisotropy of both Nd and Fe ions (see Fig. S5 in the Supplemental Material [42]). NdFeO₃ shows paramagnetic to the G -type AFM phase transition around 674 K, which is in good agreement with the experimental observation [12]. However, no second phase transition was observed here. This highlights the importance of the antisymmetric and

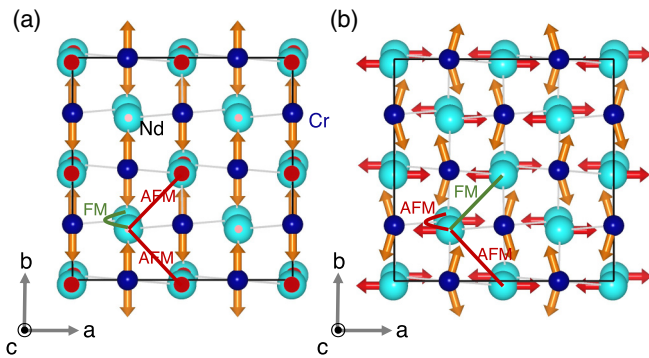


FIG. 5. (a) Experimentally proposed *C*-type magnetic ordering in the Nd sublattice [18] having *Pbnm* magnetic symmetry. Nd spins (denoted by red arrow) orient along the *z* axis. The Nd spins order in AFM and FM patterns in the (001) plane and along the [001] axis, respectively. We denote this magnetic ordering as C_{001} . (b) Proposed *C*-type magnetic ordering in the Nd sublattice through the MC simulations. Nd spins are oriented along the *x* axis. The Nd spins form AFM ordering along the [001] and [1-10] axes and FM ordering along the [110] axis. We denote this magnetic ordering as C_{110} . The Cr spins (denoted by orange arrow) are ordered in G_y pattern. The strong isotropic exchange interactions between two magnetic sublattices create a C_{110} type canted spin component in the Cr sublattice.

anisotropic-symmetric exchange interactions in the observed SR transitions in NdFeO_3 .

G. Magnetic ordering in Nd sublattice

So far, we have discussed the collective magnetic ordering in the Cr sublattice as observed at different temperatures. In this subsection we take up the case of the Nd sublattice.

The nature of the magnetic ordering corresponding to the Nd sublattice to date remains ambiguous [17,18,29]. The very existence of magnetic ordering in the Nd sublattice, as a matter of fact, is debated, given the fact the ordering must occur at very low temperature due to weak Nd-Nd interaction. The evidence of ordering of the R sublattice is normally manifested as a small λ peak in specific heat superimposed on the Schottky anomaly, the latter arising due to finite R-M interaction. In contrast to the Nd ferrite, no such λ peak is observed in the specific heat of NdCrO_3 , suggesting cooperative ordering of the Nd sublattice is prohibited [29]. Neutron diffraction study [18], on the other hand, suggests *C*-type magnetic ordering in Nd sublattices, where Nd spins are ordered in AFM and FM manners in the crystallographic (001) plane and along the crystallographic [001] axis, respectively [see Fig. 5(a)]. We denote this magnetic structure as C_{001} . However, our MC results below T_{SR} show the stabilization of a different variety of *C*-type ordering. Here, the Nd spins form AFM ordered patterns along the crystallographic [001] and [1-10] axes and an FM ordered pattern along the crystallographic [110] axis. We observe that the Nd spins are directed along the [100] axis (*x* axis) [cf. Fig. 5(b)]. We denote this magnetic ordering as C_{110} . This type of magnetic ordering is expected to break the crystal symmetry, leading to doubling of the size of the unit cell.

We need to keep a few points in mind though. The strong isotropic exchange interactions between two magnetic sublattices create a C_{110} type canted spin component in the Cr sublattice. Below T_{SR} the magnetically ordered Cr sublattice is expected to create a strong anisotropic and antisymmetric exchange field on the Nd spin. This field can compete with the SIA tendency and can influence the precise nature of spin ordering of the Nd sublattice. Our present calculation does not take into account these additional factors, which may influence the magnetic order in the Nd sublattice at low temperatures, leaving the issue open. Further investigations need to be conducted to gain a deeper insight in this regard.

IV. CONCLUSION AND DISCUSSIONS

Using a combination of first-principles calculations and finite-temperature MC simulations on a DFT derived spin Hamiltonian we studied the complex magnetism of NdCrO_3 , especially the spin reorientation transition of the Cr sublattice. The most exhaustive theoretical study on spin reorientation in rare-earth orthochromites and orthoferrites [24], given about three decades ago, was based on mean field study of the spin Hamiltonian in parameter space. While this study was successful in explaining SR of both categories (I) and (II), it failed to explain SR of category (V), i.e., that of NdCrO_3 motivating the present study. Our study importantly took into account the SIA of Nd spins, which was neglected in the study by Yamaguchi [24]. In order to gain understanding of the microscopic origin of the SR transition in NdCrO_3 , we carried out calculations switching off and on SIA of Nd spins, varying the SIA of Cr spins around the DFT estimated values, and varying the Nd-Cr exchange strength, parametrized through γ .

Our analysis established the crucial role of SIA of Nd spins in driving the SR transition, provided the Nd-Cr magnetic exchange is above a critical strength. Strengthening of Nd-Cr exchange further beyond another limit leads to cooperative ordering of the Nd sublattice avoiding the SR transition of the Cr sublattice. Further the experimentally observed nature of SR transition in NdCrO_3 was found to be reproduced only for a restricted parameter range of SIA of Cr spins, highlighting the importance of SIA of Cr spins, though it is an order of magnitude weaker in strength compared to SIA of Nd spins. Thus our findings point to the fact that SR observed in NdCrO_3 arises out of a delicate balance between Nd-Cr exchange, Nd SIA as well as Cr SIA. While the significant strength of Nd-Cr exchange and SIA of Nd spins set the stage, the SIA of Cr spins, which is an order of magnitude smaller compared to that of Nd spins, decides the details.

We would like to end our discussion with some open issues and suggestions. Our study as mentioned already did not take into account the antisymmetric and anisotropic-symmetric exchange interactions, but rather focused only on isotropic exchanges. The antisymmetric and anisotropic-symmetric exchanges in M sublattice are expected to give rise to canting and ferromagnetic component to Cr spin ordering, as observed experimentally. These exchanges between M and R sublattices were suggested to be crucial for driving SR in GdCrO_3 , for example, though they are expected to be one and two orders of magnitude smaller compared to isotropic exchanges. We note

the importance of SIA is negligible for Gd^{3+} , thus making the antisymmetric exchange of M-R interaction important. In the case of $NdCrO_3$, however, consideration of only isotropic M-R exchange in the presence of finite and moderately strong SIA of Nd spins together with weak but finite SIA of Cr spins was sufficient in capturing the SR. The effect of antisymmetric and anisotropic-symmetric exchange interactions thus would come as a secondary effect.

While our study primarily focused on SR transition, we also studied the possibility of cooperative ordering of Nd spins, which remains controversial. Our study points to a C_{110} type ordering of Nd spins, in contrast to C_{001} type ordering suggested from neutron diffraction [18]. This will be taken up in a future study involving a more complete Hamiltonian. Also it calls for further experimental studies.

Finally, it will be an interesting idea to study the SR in a mixed orthoferrite-chromite compound, $NdFe_xCr_{1-x}O_3$, given the fact that γ is about a factor of two smaller in $NdFeO_3$ compared to $NdCrO_3$; $NdFeO_3$ does not exhibit SR transition following the proposed mechanism for $NdCrO_3$. This

may make the influence of the antisymmetric and anisotropic-symmetric exchange interactions important. It is interesting to note that both high temperature and low temperature symmetry of spin ordering of the M sublattice in $NdFeO_3$ is different from that of $NdCrO_3$, it being G_x (G_z) for $NdFeO_3$ and G_z (G_y) for $NdCrO_3$ before (after) SR. To the best of our knowledge, the phase diagram of mixed compound, $NdFe_xCr_{1-x}O_3$, is yet to be explored either experimentally or theoretically. We hope our study will motivate further studies in this direction.

ACKNOWLEDGMENTS

The authors gratefully acknowledge discussion with B. Rahaman, S. Bandyopadhyay, and S. Kanthal. Research at Tokyo Institute of Technology is supported by the Grants-in-Aid for Scientific Research No. 19K05246 and No. 19H05625 from the Japan Society for the Promotion of Science (JSPS). H.D. acknowledges computational support from TSUBAME supercomputing facility. T.S.-D. acknowledges J.C.Bose National Fellowship (Grant No. JCB/2020/000004) for funding.

-
- [1] D. Treves, *Phys. Rev.* **125**, 1843 (1962).
 [2] K. W. Blazey and G. Burns, *Proc. Phys. Soc.* **91**, 640 (1967).
 [3] K. Tsushima, K. Aoyagi, and S. Sugano, *J. Appl. Phys.* **41**, 1238 (1970).
 [4] R. L. White, *J. Appl. Phys.* **40**, 1061 (1969).
 [5] Y. Tokunaga, S. Iguchi, T. Arima, and Y. Tokura, *Phys. Rev. Lett.* **101**, 097205 (2008).
 [6] B. Rajeswaran, D. I. Khomskii, A. K. Zvezdin, C. N. R. Rao, and A. Sundaresan, *Phys. Rev. B* **86**, 214409 (2012).
 [7] Y. Tokunaga, N. Furukawa, H. Sakai, Y. Taguchi, T. Arima, and Y. Tokura, *Nat. Mater.* **8**, 558 (2009).
 [8] H. J. Zhao, L. Bellaiche, X. M. Chen and J. Íñiguez, *Nat. Commun.* **8**, 14025 (2017).
 [9] X. Ye, J. Zhao, H. Das, D. Sheptyakov, J. Yang, Y. Sakai, H. Hojo, Z. Liu, L. Zhou, L. Cao, T. Nishikubo, S. Wakazaki, C. Dong, X. Wang, Z. Hu, H.-J. Lin, C.-T. Chen, C. Sahle, A. Efiminko, H. Cao *et al.*, *Nat. Commun.* **12**, 1917 (2021).
 [10] M. Marezio, J. P. Remeika, and P. D. Dernier, *Acta Crystallogr.* **B26**, 2008 (1970).
 [11] M. C. Weber, J. Kreisel, P. A. Thomas, M. Newton, K. Sardar, and R. I. Walton, *Phys. Rev. B* **85**, 054303 (2012).
 [12] D. Treves, *J. Appl. Phys.* **36**, 1033 (1965).
 [13] S. Artyukhin, M. Mostovoy, N. P. Jensen, D. Le, K. Prokes, V. G. de Paula, H. N. Bordallo, A. Maljuk, S. Landsgesell, H. Ryll, B. Klemke, S. Paegel, K. Kiefer, K. Lefmann, L. T. Kuhn, and D. N. Argyriou, *Nat. Mater.* **11**, 694 (2012).
 [14] S. J. Yuan, W. Ren, F. Hong, Y. B. Wang, J. C. Zhang, L. Bellaiche, S. X. Cao, and G. Cao, *Phys. Rev. B* **87**, 184405 (2013).
 [15] Z. Y. Zhao, X. Zhao, H. D. Zhou, F. B. Zhang, Q. J. Li, C. Fan, X. F. Sun, and X. G. Li, *Phys. Rev. B* **89**, 224405 (2014).
 [16] E. F. Bertaut, J. Mareschal, G. de Vries, R. Aleonard, R. Pauthenet, J. P. Rebouillat, and J. Sivardiere, *IEEE Trans. Magn.* **2**, 453 (1966).
 [17] F. Bartolomé, J. Bartolomé, M. Castro, and J. J. Melero, *Phys. Rev. B* **62**, 1058 (2000).
 [18] N. Shamir, H. Shaked, and S. Shtrikman, *Phys. Rev. B* **24**, 6642 (1981).
 [19] E. F. Bertaut and J. Mareschal, *Solid State Commun.* **5**, 93 (1967).
 [20] H. J. Zhao, J. Íñiguez, X. M. Chen, and L. Bellaiche, *Phys. Rev. B* **93**, 014417 (2016).
 [21] J. P. Bolletta, F. Pomiro, R. D. Sánchez, V. Pomjakushin, G. Aurelio, A. Maignan, C. Martin, and R. E. Carbonio, *Phys. Rev. B* **98**, 134417 (2018).
 [22] M. Taheri, F. S. Razavi, Z. Yamani, R. Flacau, C. Ritter, S. Bette, and R. K. Kremer, *Phys. Rev. B* **99**, 054411 (2019).
 [23] I. Fita, R. Puzniak, and A. Wisniewski, *Phys. Rev. B* **103**, 054423 (2021).
 [24] T. Yamaguchi, *J. Phys. Chem. Solids* **35**, 479 (1974).
 [25] E. Bousquet and A. Cano, *J. Phys.: Condens. Matter* **28**, 123001 (2016).
 [26] I. Dzyaloshinski, *J. Phys. Chem. Solids* **4**, 241 (1958).
 [27] T. Moriya, *Phys. Rev.* **120**, 91 (1960); in *Magnetism I*, edited by G. T. Rado and H. Suhl (Academic Press, New York, 1963), p. 85.
 [28] R. M. Hornreich, Y. Komet, R. Nolan, B. M. Wanklyn, and I. Yaeger, *Phys. Rev. B* **12**, 5094 (1975).
 [29] F. Bartolomé, M. D. Kuzmin, J. Bartolomé, J. Blasco, J. García, and F. Sapiea, *Solid State Commun.* **91**, 177 (1994).
 [30] J. Ramesh, N. Raju, S. Shravan Kumar Reddy, M. Sreenath Reddy, Ch. Gopal Reddy, P. Yadagiri Reddy, K. Rama Reddy, and V. Raghavendra Reddy, *J. Alloy Compd.* **711**, 300 (2017).
 [31] R. M. Hornreich, *J. Magn. Magn. Mater.* **7**, 280 (1978).
 [32] B. Ayasse, A. Berton, and J. Sivardière, *C. R. Acad. Sci. Paris B* **271**, 1220 (1970).
 [33] P. Blaha, K. Schwarz, G. K. H. Madsen, D. Kvasnicka, J. Luitz, R. Laskowski, F. Tran, and L. D. Marks, WIEN2k: An augmented plane wave plus local orbitals program for calculating crystal properties, Vienna University of Technology, Austria, 2018, <http://www.wien2k.at/index.html>.

- [34] P. Blaha, K. Schwarz, F. Tran, R. Laskowski, G. K. H. Madsen, and L. D. Marks, *J. Chem. Phys.* **152**, 074101 (2020).
- [35] J. P. Perdew, K. Burke, and M. Ernzerhof, *Phys. Rev. Lett.* **77**, 3865 (1996).
- [36] V. I. Anisimov, I. V. Solovyev, M. A. Korotin, M. T. Czyżyk, and G. A. Sawatzky, *Phys. Rev. B* **48**, 16929 (1993).
- [37] P. H. Dederichs, S. Blügel, R. Zeller, and H. Akai, *Phys. Rev. Lett.* **53**, 2512 (1984).
- [38] V. I. Anisimov, J. Zaanen, and O. K. Andersen, *Phys. Rev. B* **44**, 943 (1991); W. E. Pickett, S. C. Erwin, and E. C. Ethridge, *Phys. Rev. B* **58**, 1201 (1998).
- [39] N. Metropolis and S. Ulam, *J. Am. Stat. Assoc.* **44**, 335 (1949).
- [40] N. Metropolis, A. W. Rosenbluth, M. N. Rosenbluth, and A. H. Teller, *J. Chem. Phys.* **21**, 1087 (1953).
- [41] J. Prado-Gonjal, R. Schmidt, J.-J. Romero, D. Ávila, U. Amador, and E. Morán, *Inorg. Chem.* **52**, 313 (2013).
- [42] See Supplemental Material at <http://link.aps.org/supplemental/10.1103/PhysRevMaterials.5.124416> for (i) the calculated values of superexchange interactions between magnetic ions and relative magnetic anisotropy energy (MAE) of the magnetic ions, as a function of J_H and U , (ii) modulation of the magnetic order parameters of the Cr sublattice as a function of temperature and γ , and (iii) magnetic behavior of NdFeO₃.